Implementation of a FPGA-based data acquisition and processing system for image sensors employed in SPR biosensing

Eduardo G. Pereira*†, Leiva C. Oliveira*†, Marcos R.A. Morais*, Antonio M.N. Lima*, and H. Neff*
*Department of Electrical Engineering - DEE, Universidade Federal de Campina Grande - UFCG
Rua Aprígio Veloso, 882, 58429-900, Bairro Universitário, Campina Grande, Paraíba, Brazil
†Programa de Pós-Graduação em Engenharia Elétrica, PPgEE, UFCG, Brazil
e-mail: {eduardo.pereira, leiva.oliveira}@ee.ufcg.edu.br, {morais, amnlima}@dee.ufcg.edu.br, heneff@web.de

***Abstract*—Optical biosensors based on surface plasmon resonance (SPR) are powerful tools for detecting biomolecules. In this paper, a reconfigurable image acquisition and processing system for SPR sensors is presented. The system uses a FPGA device for acquiring and processing data from an image sensor to determine the angle at which the minimum reflectivity of the optical multilayer arrangement occurs. A frequency domain processing for smoothing the SPR signal is implemented in hardware. The system also incorporates a communication interface for sending processed and unprocessed data from the FPGA to a remote device and receiving settings regarding the data acquisition and data processing strategies.**

***Keywords*—biosensor, data acquisition system, FPGA, surface plasmon resonance**

I. Introduction

Surface Plasmon Resonance (SPR) sensors are used for detection, identification and quantification of biomolecular interactions. Presently, SPR biosensors can be found in a broad range of applications [1], [2]. The SPR devices are mostly built under the Kretschmann configuration, with SPR phenomenon excitation with light under attenuated total reflection (ATR). In this configuration, the SPR device monitors the reflected light intensity at a specific angle or wavelength to track the substance of interest [3].

The image sensor plays a fundamental role in SPR sensing and, together with the other optical components, dictate the final sensitivity and noise characteristics of the equipment. Nonetheless, the raw data extracted from the equipment is very noisy and should be processed using smoothing techniques for further use by other data processing algorithms. Usually, commercial cameras with USB or Ethernet connections are used in SPR equipments. For that, a computer performs signal processing like curve smoothing, curve generation and parameters extraction. It is possible to find SPR instruments based on smartphone [4], FPGA [5], and microcontrollers [6].

Such arrangement may support the implementation of super-resolution techniques [7], low latency frequency analysis, and other computationally intensive operations. The advantages of using a custom designed controller include, for instance, fine control of the sensor integration time, sensor raw data acquisition with all available bits, selection of an area of interest and multi-spot acquisition capabilities. Some other practical aspects include the form factor of the sensor, which can be tailored to fit in the overall optical project. In addition, the lower level interface with the camera sensor, including out of image pixels, allows the implementation of self-calibration and diagnostic techniques.

In this paper, an image acquisition and processing system for SPR sensor applications is presented. The system uses an FPGA device for control, acquisition and data processing for a CMOS S11661 image sensor [8]. An efficient processing system enabling high noise immunity and low latency was developed. A communication interface has also been integrated, enabling the sending of processed and unprocessed data and configuration strategies for acquisition (i.e. integration time, image size) and processing (i.e. filter parameters).

II. SPR biosensing

SPR is a well-established method for real-time, label-free monitoring of molecular interactions. The phenomenon occurs in thin conducting films at an interface between media of different refractive index. In a typical SPR biosensor, the media are a supporting optical prism and a sample solution. Both media are equally treated as dielectric materials, but typically exhibit different dielectric functions. The conducting film is usually a thin layer of gold or silver. A simplified representation of the multilayered SPR system is shown in Fig. 1.

Under total internal reflection condition and at a certain combination of light incidence angle and wavelength, the incident light, k_x, excites surface plasmon (electron charge density waves) in the metal film. Thus, an electric field intensity leaks across metal/dielectric interface, the so-called evanescent wave field, making this resonance effect very sensitive to the refractive index of the solution within the effective penetration depth of the evanescent field.

The surface plasmon wave vector can be mathematically approximated by [9]

978-1-4673-6386-0/14/$31.00 ©2014 IEEE

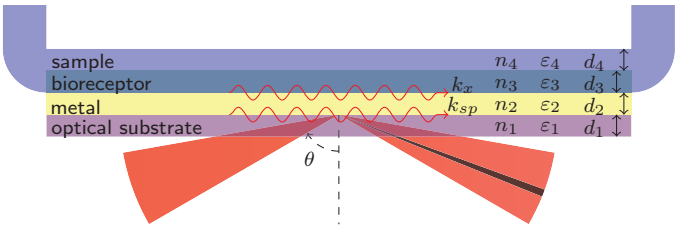

Fig. 1: Multilayer SPR biosensor structure representation. The surface plasmon vector k_{sp} resonates with the evanescent field k_x, resulting in reflectivity reduction as indicated by the black stripe observed at the reflected light beam.

$$k_{sp} = \frac{2\pi}{\lambda}\sqrt{\frac{\varepsilon_{2r} n_3^2}{\varepsilon_{2r} - n_3^2}} \tag{1}$$

where k_{sp} depends on the real part of the dielectric constant of the metal ε_{2r}, the refractive index of the medium n_3, and the incident light wavelength λ.

The k_x component depends on the refractive index of the dispersive medium n_1, the angle of incidence θ and the incident light wavelength λ, expressed by [9]

$$k_x = \frac{2\pi}{\lambda} n_1 \sin\theta \tag{2}$$

The resonance condition means that k_x vector oscillates with the same frequency and amplitude of the surface plasmon wave. As a result, a characteristic absorption of energy occurs and SPR is seen as a drop in the intensity of the reflected light at a specific angle of incidence θ_{RES}, called the resonance angle (see Fig. 2). The SPR sensing concept essentially consists of monitoring the resonance angle and compute the refractive index n_3 of the interest substance by

$$n_3 = \sqrt{\frac{\varepsilon_{2r}(n_1 \sin\theta_{\text{RES}})^2}{\varepsilon_{2r} - (n_1 \sin\theta_{\text{RES}})^2}} \tag{3}$$

The refractive index of the sensitive medium n_3 changes as new substances are admitted to the flow cell; n_3 changes means a change in the resonance angle and the graphs of its values over time is called sensorgram.

III. System Design

A. Optical Configuration

Usually, surface plasmon resonance biosensors requires a relatively complex structure. This structure comprises optical, mechanical, fluidic, electronic and thermal elements. The basic configuration of the proposed SPR biosensing system is shown in Fig. 3. It includes of a source of monochromatic light ($\lambda = 670nm$) with associated collimating lens, so that all light rays are parallel. A polarizer allowing the passage of light in a unique polarization, i.e., parallel to the plane of incidence. A Diffractive Optical Coupling Element (DOCE), upon which a metal film is deposited, acts as a waveguide that directs light to the

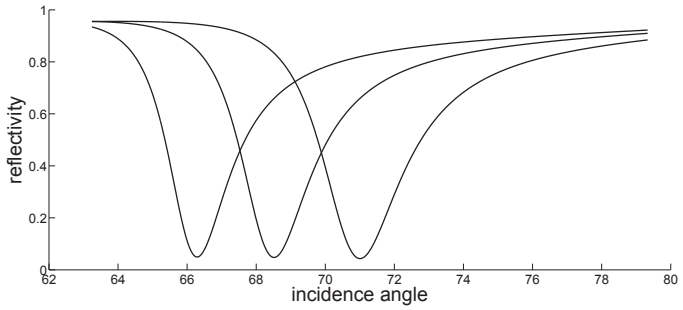

Fig. 2: Reflectivity in function of incidence angle for three different sample solutions (n_4). The minimum reflectance is the resonance conditions that shifts when the sample solution changes.

central region where the transducer element is located [9]. A peristaltic pump pumps the solution to the sensitive spot located at central region and the optical detector and imaging processing system, which is the focus of this work, performs all the tasks to bring a clean image or measured characteristics to the user or host device. The monochromatic light generated by the laser diode passes through the collimating and polarizing lens so that the light beam is perpendicular to the DOCE surface. Due to the diffracting grating that light is split and will hit the sensing spot at different incident angles. The light reflected at the sensing spot also goes through a similar diffracting grating such that the outgoing light rays are parallel and are captured by the image sensor.

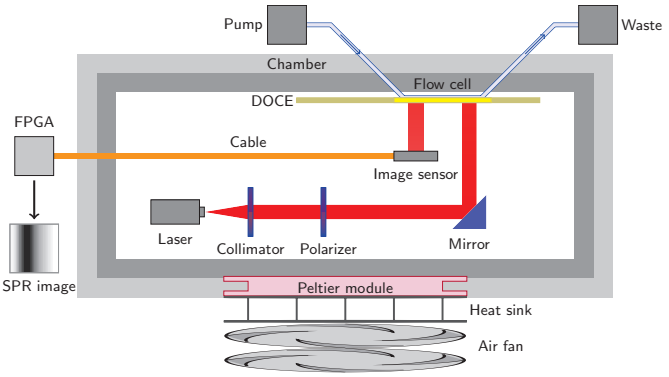

Fig. 3: Basic structure of the proposed SPR biosensing system.

In a SPR system, some external factors contribute to increase the noise-level such as ambient light and temperature. Ambient illumination can interfere in the determination of the surface reflectivity due to ambient light that hits the optical detector. Changes in temperature affect the refractive index of aqueous solutions and the sensitivity of the SPR sensor [10]. Also, some biochemical interactions, as antibody-antigen binding, can be optimized at specific temperature conditions [11]. The multilayer structure is placed into an optical and thermal isolated chamber (8cm height; 10cm length; and 6cm depth) to preserve the performance by reducing the effects of the

external factors that contribute to increase the noise-level. A thermoelectric module connected to an air fan controls the chamber internal temperature in order to stabilize the device sensibility, improve the immunity to temperature changes and optimize some biochemical interactions.

B. Hardware Architecture

A simplified block diagram of the image sensor interface architecture can be seen in Fig. 4. The elements that compose such architecture are enough to effectively perform all the required processing operations of a SPR sensing system. The red (image sensor and SDRAM) and green (Host) blocks correspond to elements that are external to the FPGA chip. The image sensor captures the image and the memory can be used as auxiliary buffer to assist in the processing, depending on the configuration. The red lines represent the acquired data flow and the black lines represent control, addressing and status signals.

All blocks were designed in reconfigurable logic, using the Verilog hardware description language [12]. The proposed circuit has been implemented on a Cyclone II EP2C35F672C6N FPGA device produced by Altera. The Verilog HDL code has been synthesized using Quartus II software, with the default settings. The FPGA resources usage obtained after compilation are presented in Table I.

TABLE I: Resource Usage Compilation Results

Resource	Usage
Logic elements	16124
Memory bits	409600
Embedded Multipler 9-bit	48

The system operates at 50MHz clock rate and there are three main operation modes: two dimensions with filtering (**2DF**); one dimension with filtering (**1DF**); and without filtering (**WF**). In the **2DF** mode, the obtained image filtering is performed on each row and in each column subsequently. In the **1DF** mode, the obtained image filtering is performed only on each row. In the **WF** mode, the obtained data is send directly to an external device, without filtering process.

Through the communications interface, the user is allowed to choose the operating mode of the system, as well as the filter properties (gain of each component of the Fourier expansion) and the data acquisition parameters of the image sensor. The user configurations are sent to the control unit, which implements the configuration of each block. The control unit also implements the processes of synchronization of all units, generating control signals and data addressing.

The SPI communication interface controls the transmission of the configuration of several parameters of the image sensor. Some parameters that can be configured are: the integration time, that is, the time that light accumulates on the sensor; the gain of the A/D (Analog-to-Digital) converter; and the desired area for image acquisition; selection of the sensing area is quite important for allowing multi-spot sensing.

The single line buffers have a storage capacity of 1024x12-bit pixels and are used in the data acquisition and image processing steps. The buffers are required due to different transmission rates between the image sensor and the DFT blocks and between the IDFT and the SDRAM (Synchronous dynamic random access memory) blocks. The memory control block simplifies the access to SDRAM through synchronization and automatic generation of refresh cycles.

The data filtering process is performed on the yellow shaded part (A). The DFT and IDFT blocks performs direct and inverse Fourier transforms, respectively. Those blocks are based on the DFT/FFT IP Generator [13] of the Spiral Project [14].

C. FPGA Data Flow and Processing

The image sensor transmit one pixel at every 4 clock pulses. A signal is sent from the image sensor to the control unit when the pixels of one row starts to be transmitted. At this time, the image sensor buffer input addressing is reset. At arrival of every new pixel, the image sensor buffer input addressing is incremented. After one full-row is transmitted, there is a wait interval of 480 clock pulses until the next row is transmitted. Similarly, a signal is sent to inform the start of a full image transmission. There is a parameterized wait interval between full image transmissions.

When the image sensor buffer is full, its data are transmitted to the DFT block at 4 pixels per pulse clock rate, using the wait time between the end and start transmission time from image sensor. When the DFT block finishes the Fourier Transform, it sends a status signal to the control unit and the transformed data are transmitted to the filter block at 4 pixels per pulse clock rate. Upon reaching the filter block, each one of the Fourier components is attenuated or amplified according to the user configuration filter parameter choices and, at the same time, transferred into the IDFT block. Similarly, when the IDFT block finishes the Inverse Fourier Transform, it sends a status signal to the control unit and the transformed data are transmitted to the filter buffer at 4 pixels per pulse clock rate.

From the filter buffer, the filtered data are transmitted to the SDRAM through the memory control block at 1 pixel per pulse clock rate. The SDRAM retains the data until one full image is saved. After that, the memory transmits each column from the image through the memory buffer to pass through the filter part (A) using the time that the image sensor buffer is being filled. At this time, the data are transmitted to the communication interface, from which it is transmitted to an external device.

In the **WF** mode, the data are directly transmitted from the image sensor buffer to the communication interface, without passing trhough the filter (A) and memory (B) parts. In the **1DF** mode, the data are directly transmitted from the filter buffer to the communication interface, without using the memory. To save energy, the memory is turned off when operating at **1DF** mode, and

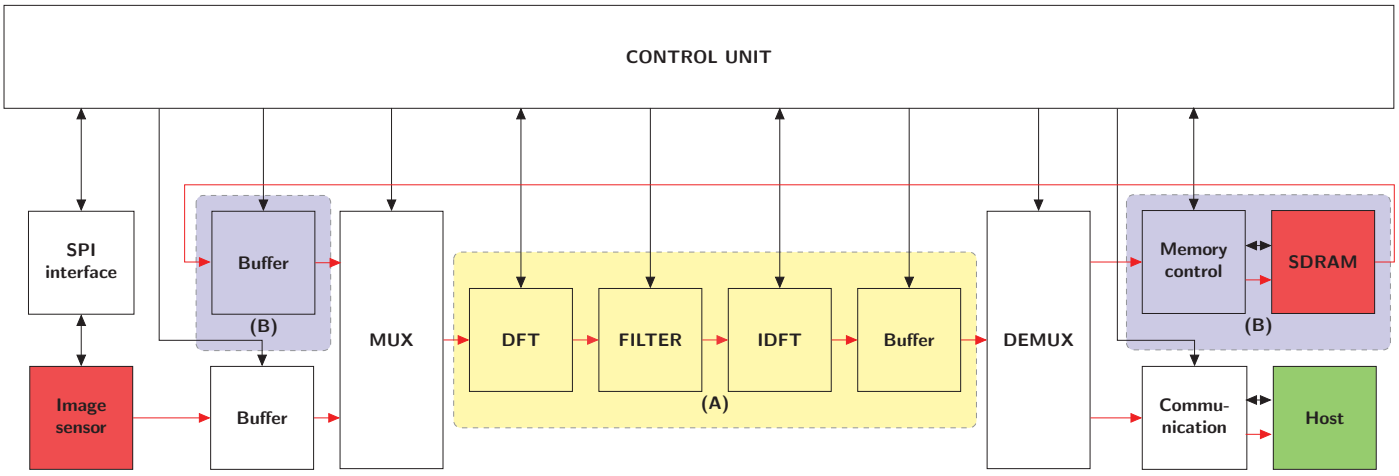

Fig. 4: Simplified block diagram of the image sensor interface architecture. The red lines represent the data flow and the black lines denote control signals.

both the filter and memory are turned off when operating at **WF** mode.

Upon reaching the communication interface, the data are sent uninterruptedly to the output interface. The sending protocol establishes that the data is transmitted in 16-bit packets, where the first four bits are used for control and status and the other 12 bits are allocated to pixel values. By the basic configuration, the system transmits images to external devices at 8 frames/second rate.

During the configuration, the data packet consists of one 128-bits word containing all acquisition and processing configuration parameters. The received configurations are applied to the system only when the current image ends its acquisition.

IV. Experimental Results

Photographs of the developed system (represented in Fig. 3) are presented in Fig. 5. The setup uses the SPR chip developed by Thirstrup et al. [9] for surface plasmon excitation. A DE2 Board from Terasic/Altera was used for the experimental tests. The image sensor is connected to the FPGA board through one 40-pin header and an adapter board. The FPGA board is connected through a RS-232 serial interface to a computer to show and analyze acquired data.

The experiments were performed at illumination and temperature controlled conditions. The light source (λ = 670nm laser) and the S11661 image sensor are placed inside a thermally stabilized chamber with a thermoelectric module. Samples of water (H_2O); phosphate buffered saline (PBS); and sodium hypochlorite (NaClO) solution have been pumped to the flow cell for surface plasmon resonance generation and refractive index determination.

In Fig. 6, are shown the filtered obtained images from H_2O; PBS; and NaClO. Its extracted SPR curves are shown in Fig. 7. To determine the minimum reflectivity position, the pixel number corresponding to the minimum intensity, p_{min}, is determined by the centroid method

$$p_{min} = \frac{\sum_{p=p_{initial}}^{p_{final}} pI_B - pI[p]}{\sum_{p=p_{initial}}^{p_{final}} I_B - I[p]}, \quad (4)$$

where: I_B is the specified base line; p is pixel number; $I[p]$ is the intensity of the p^{th} pixel; and p_{inital} and p_{final} are the pixel numbers defining the start and the end of the analysis region.

The pixel position corresponding to the minimum intensity, p_{min}, can be converted in terms of resonance angle, θ_{RES}, based on geometrical relationships determined by the physical arrangement of the image sensor and pixel size. The pixel-angle conversion equation is

$$\theta_{RES} = \theta_0 + p_{min}\Delta\theta \quad (5)$$

where: θ_0 is the angle from the first pixel (index 0); and $\Delta\theta$ correspond to the pixel-angle relation. In the current system, $\theta_0 = 65.577$ degrees; and $\Delta\theta = 0.0055$ degrees.

The resonance angle is used to determine the substance refractive index n_3 based on (3) with $n_1 = 1.526$ and $\varepsilon_{2r} = -13.3$ [9]. The experimental values obtained from minimum pixel position; resonance angle; and refractive index for H_2O; PBS; and NaClO solution are presented in Table II.

TABLE II: Experimental values obtained from minimum pixel position; resonance angle; and refractive index for H_2O; PBS; and NaClO solution.

Substance	p_{min}	θ_{res}	n_3
H_2O	556	68.6375	1.3242
PBS	576	68.7475	1.3250
NaClO	736	69.3550	1.3297

V. Conclusions

In this paper, the development of a image acquisition and processing system based on FPGA for SPR sensing ap-

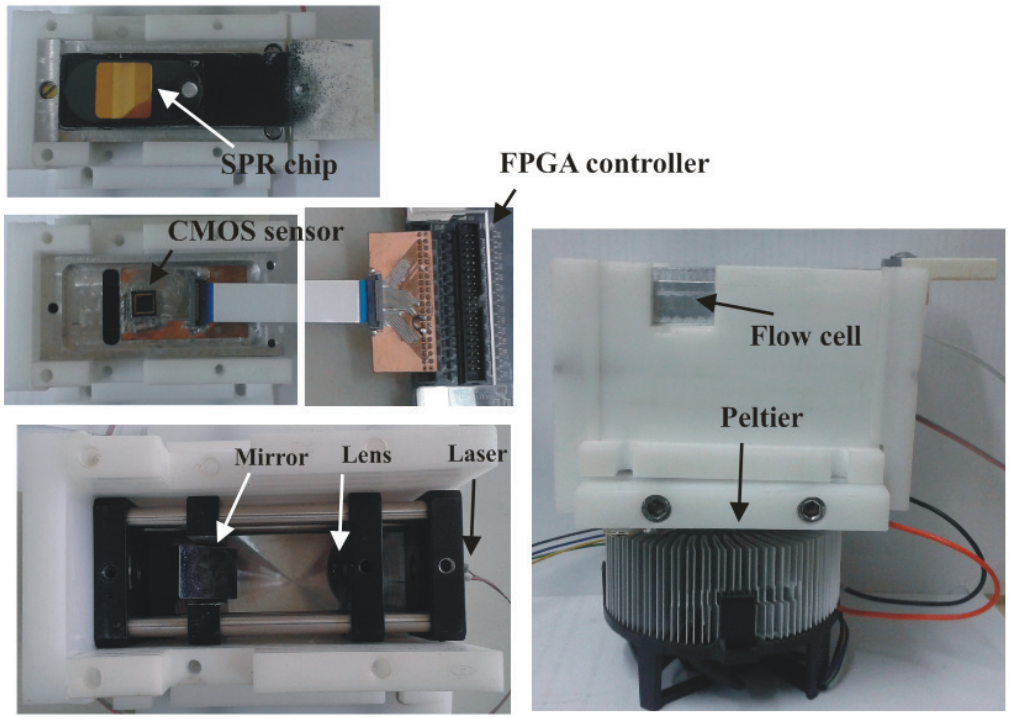

Fig. 5: Photographs of the developed prototype system. Labels on the photographs indicate the system components.

(a) (b) (c)

Fig. 6: Experimental images obtained from (a) H_2O; (b) PBS solution; and (c) NaClO solution.

plication was presented. The developed system integrates good strategies for conditioning and processing the acquired signals to obtain more accurate results. In addition, the system enables a good acquisition speed. The system enables the user to control the strategies of conditioning and signal processing. A communication interface for data transmission has also been developed. Experimental results were presented to show the operation of the system.

Acknowledgment

The authors thank to PPgEE-UFCG, DEE-UFCG, CAPES and CNPq for the award of research grants and study fellowship during the course of these investigations. A special thank to Simões Toledo for his aid in the PCB manufacturing.

References

[1] D. G. Myszka and R. L. Rich, "Implementing surface plasmon resonance biosensors in drug discovery," *Pharmaceutical Science & Technology Today*, vol. 3, no. 9, pp. 310 – 317, 2000.

[2] D. Yeung, A. Gill, C. Maule, and R. Davies, "Detection and quantification of biomolecular interactions with optical biosensors," *TrAC Trends in Analytical Chemistry*, vol. 14, no. 2, pp. 49 – 56, 1995.

[3] J. Homola, S. S. Yee, and G. Gauglitz, "Surface plasmon resonance sensors: review," *Sensors and Actuators B: Chemical*, vol. 54, no. 1–2, pp. 3 – 15, 1999.

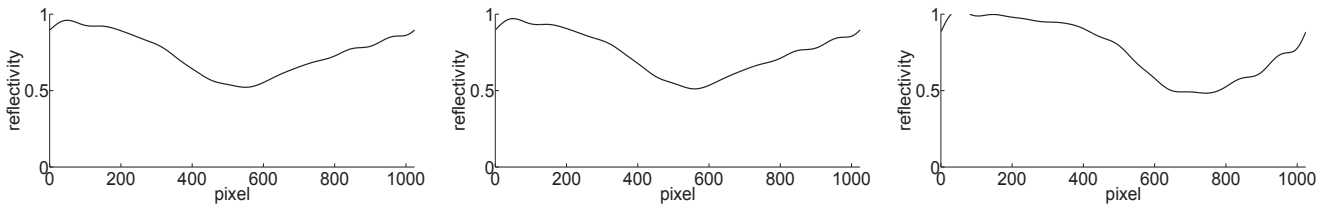

(a) (b) (c)

Fig. 7: Experimental SPR curves extracted from the images from Fig. 6. SPR curves obtained from (a) H_2O; (b) PBS solution; and (c) NaClO solution.

[4] P. Preechaburana, M. C. Gonzalez, A. Suska, and D. Filippini, "Surface plasmon resonance chemical sensing on cell phones," *Angewandte Chemie International Edition*, vol. 51, no. 46, pp. 11585–11588, 2012.

[5] F. Weichert, M. Gaspar, C. Timm, A. Zybin, E. Gurevich, M. Engel, H. Müller, and P. Marwedel, "Signal analysis and classification for surface plasmon assisted microscopy of nanoobjects," *Sensors and Actuators B: Chemical*, vol. 151, no. 1, pp. 281 – 290, 2010.

[6] J. Hu, J. Hu, F. Luo, W. Li, G. Jiang, Z. Li, and R. Zhang, "Design and validation of a low cost surface plasmon resonance bioanalyzer using microprocessors and a touch-screen monitor," *Biosensors and Bioelectronics*, vol. 24, no. 7, pp. 1974 – 1978, 2009.

[7] W. Freeman, T. Jones, and E. Pasztor, "Example-based super-resolution," *Computer Graphics and Applications, IEEE*, vol. 22, no. 2, pp. 56–65, 2002.

[8] Hamamatsu Photonics, *Prototype Specification Sheet CMOS area image sensor TYPE No. S11661*, 2012.

[9] C. Thirstrup, W. Zong, M. Borre, H. Neff, H. Pedersen, and G. Holzhueter, "Diffractive optical coupling element for surface plasmon resonance sensors," *Sensors and Actuators B: Chemical*, vol. 100, no. 3, pp. 298 – 308, 2004.

[10] C. Moreira, A. Lima, H. Neff, and C. Thirstrup, "Temperature-dependent sensitivity of surface plasmon resonance sensors at the gold–water interface," *Sensors and Actuators B: Chemical*, vol. 134, no. 2, pp. 854 – 862, 2008.

[11] G. Zeder-Lutz, E. Zuber, J. Witz, and M. H. V. Regenmortel, "Thermodynamic analysis of antigen–antibody binding using biosensor measurements at different temperatures," *Analytical Biochemistry*, vol. 246, no. 1, pp. 123 – 132, 1997.

[12] "Ieee standard verilog hardware description language," *IEEE Std 1364-2001*, 2001.

[13] P. A. Milder, J. C. Hoe, and M. Püschel, "Automatic generation of streaming datapaths for arbitrary fixed permutations," in *Design, Automation and Test in Europe (DATE)*, pp. 1118–1123, 2009.

[14] "Spiral project." http://spiral.net/.